

2.1 Hyaline Cartilage

The hyaline articular cartilage appears remarkably smooth, both macroscopically and on examination by light microscopy (LM) or transmission electron microscopy (TEM), and even – after introduction of the cold stage – in the scanning electron microscope (Hunter 1743; Davies et al. 1962; Ghadially and Roy 1969; Draenert and Draenert 1979; Draenert et al. 2002). Hyaline cartilage is firmly anchored in the bony baseplate which is best demonstrated in histological studies with sections which have been processed under load (Fig. 2.1). Undulations, pits, and humps as surface characteristics are considered artifacts by drying (Clarke 1971a, b, c; Ghadially et al. 1976, 1977; Draenert and Draenert 1979; Draenert et al. 2002).

A tissue such as hyaline cartilage, which contains up to 70% water and which is known to easily lose proteoglycans during processing (Cameron et al. 1976), is best investigated in the frozen, non-dehydrated state (Draenert et al. 2002; Fig. 2.2). The water content of cartilage ranges from 65% to over 80% in the upper layers facing the joint (Venn and Maroudas 1977). Rosenberg et al. (1970, 1975) developed macromolecular models of protein polysaccharides. Articular cartilage may be considered as a visco- or poro-elastic fiber-composite material (Becerra et al. 2010). Recent studies on the friction coefficient of articular cartilage showed that the main boundary lubricant is the SZP molecule, the Superficial Zone Protein (Chan et al. 2010).

The scanning electron microscope probably best shows the three-dimensional structure of the tissue. A layer of ground substance free of fibers

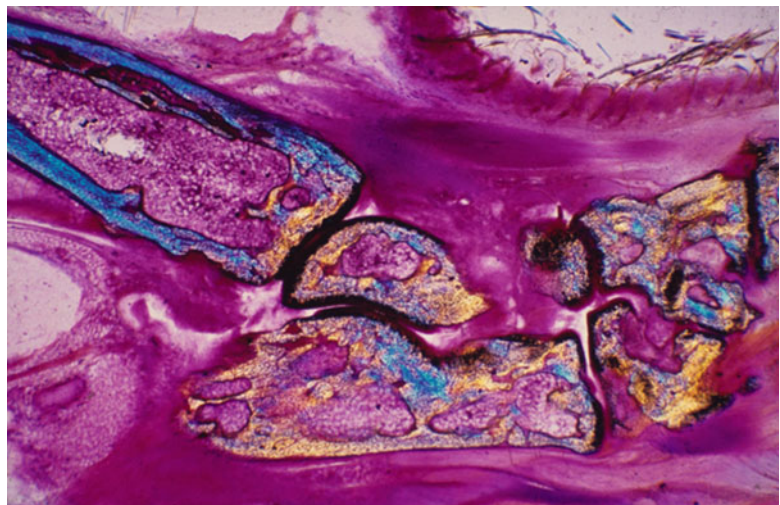


Fig. 2.1 Longitudinal section of a mouse's ankle and foot under load: the cartilage is firmly anchored with its fibers onto the bony baseplate

Fig. 2.2 Cold stage, developed in the ZOW Munich in order to study cartilage in a “nondehydrated” stage (DFG support)

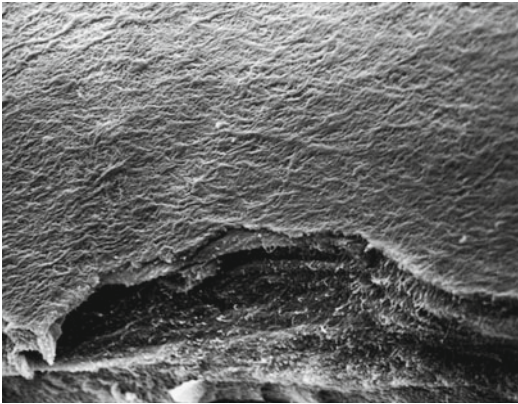
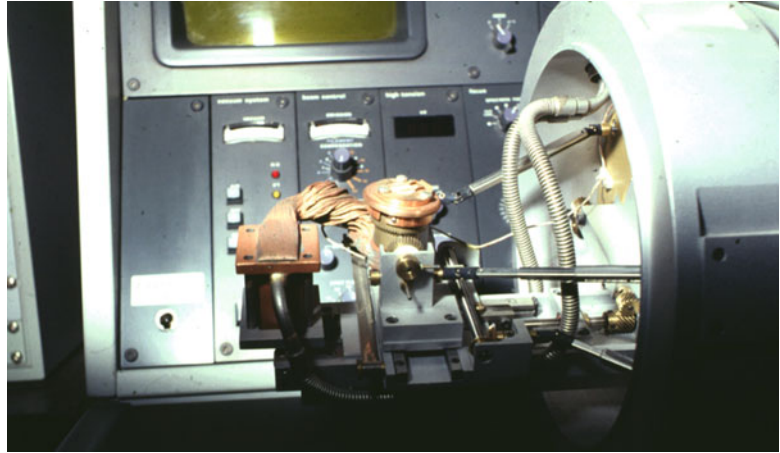


Fig. 2.3 View of the hyaline cartilage: It is smooth, without undulations, pits, and humps, revealing a lamina splendens. SEM of a freeze-dried, freeze-fractured femoral head of a rat in the PSEM 500, 25 kV, 200 Å Au. Horizontal field width=40 µm

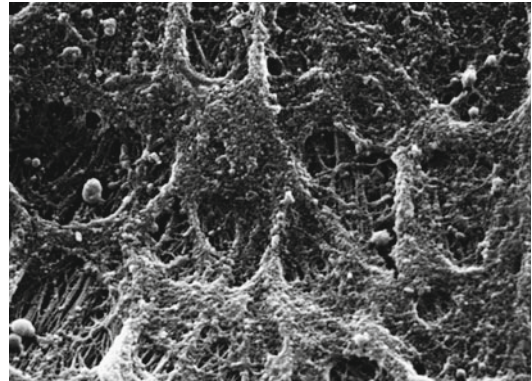


Fig. 2.4 Partially freed-fiber pattern of the tangential fiber layer of a rat's femoral head. Ice crystal processing: there is a well-organized, tangentially oriented fiber pattern visible. SEM of a freeze-dried specimen in the PSEM 500, 25 kV, 200 Å. Horizontal field width=12 µm

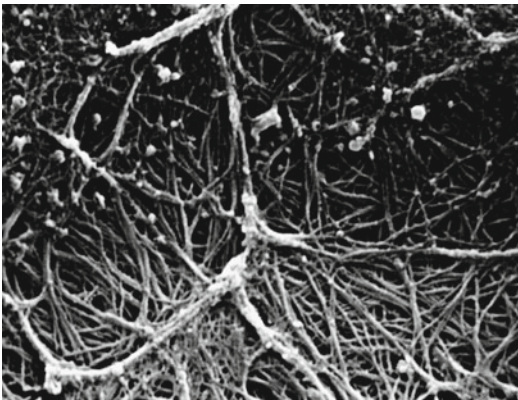


Fig. 2.5 Exposed fibers of the tangential layer of hyaline cartilage of a rat's femoral head. Ice crystal processing: there is a well-organized, tangentially oriented fiber pattern visible. A canal system is revealed through the fiber pattern. SEM of a freeze-dried specimen in the PSEM 500, 25 kV, 200 Å. Horizontal field width=12 µm

covers the surface (*lamina splendens*) (Fig. 2.3). In the electron microscope, it is revealed that the ground substance is grouted over a tangential network of collagenous fibers (Figs. 2.4 and 2.5).

The tangential layer of fibers was arched like a dome over the underlying structures. Under this dome, cell columns arched revealing disklike cells adjacent to the tangential fiber layer. Specimen processed at the cold stage showed no shrinkage at all (Fig. 2.6). In the arch, oval cells appear followed by isogenous cell groups (Figs. 2.7 and 2.8).

The surface of the cartilage baseplate is tremendously enlarged and best presented in the scanning electron microscope (Fig. 2.9).

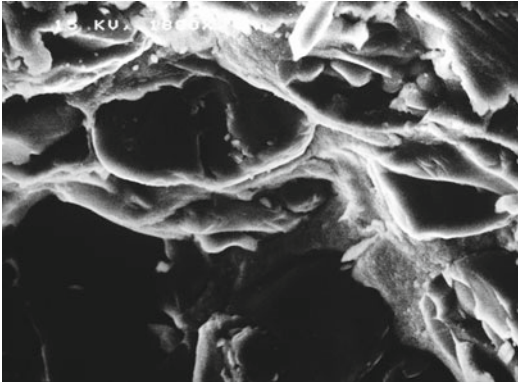


Fig. 2.6 Tangential cell layer in a nondehydrated stage: There is no shrinkage at all. The chondrocytes fill the fiber basket completely and act as hydraulic elements. SEM of a frozen nondehydrated specimen in the PSEM 500, equipped with a cold stage, 25 kV, 200 Å. Horizontal field width=35 µm

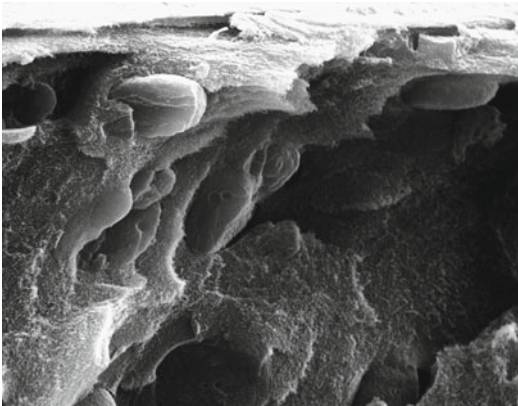


Fig. 2.7 Cell arch in a freeze-dried and freeze-fractured sample of a rat's femoral head in the SEM. The cell membrane is slightly folded due to the drying process. SEM of a freeze-dried specimen in the PSEM 500, 25 kV, 200 Å. Horizontal field width=60 µm



Fig. 2.8 Isogenous cell group of the deeper layer in a freeze-dried and freeze-fractured sample of a rat's femoral head in the SEM. Between cell membrane and fiber basket, a slight gap has developed due to the drying process. SEM of a freeze-dried specimen in the PSEM 500, 25 kV, 200 Å. Horizontal field width=35 µm

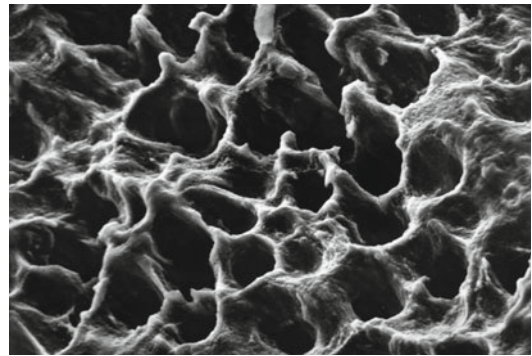


Fig. 2.9 View of the bony cartilage baseplate: A huge surface enlargement with deep pits is revealed. SEM of an air-dried specimen of a rat's femoral head corroded with Na_2O_2 and documented in the PSEM 500, 25 kV, 200 Å. Horizontal field width=80 µm

2.2 Epiphyseal Cancellous Bone

The tissue of the epiphyses consists of hyaline cartilage connected with the perichondrium to the diaphyseal tube, forming in between the growth plate and toward the perichondrium the “enchoche d’ossification” Ranvier (1873). Genetically determined, a vascularized connective tissue grows in from the perichondrium and forms the ossification center in the middle of the epiphysis (Schenk 1978). The enchondral ossification grows radially, forming the load-bearing epiphyseal joint component.

The epiphysis is comprised of the compact cartilage baseplate – cementing all fiber bundles of the hyaline cartilage – and the cancellous bone with strong arches of bone forming a vault (Fig. 2.10). Depending on the load acting on it, the cartilage baseplate can be thin, containing thin arches of cancellous bone, i.e., in the epiphyseal part of the phalanges (Fig. 2.11), or very compact, as revealed in the femoral head (Fig. 2.12). In all cases, the strength of the lamellae depends upon the load acting on it; based on Wolff’s Law (1892), an interpretation of the architecture of the cancellous bone, i.e., through

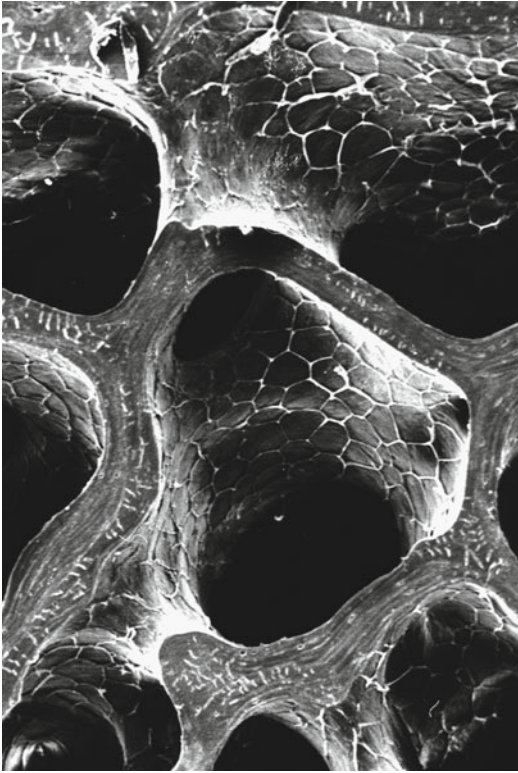


Fig. 2.10 Epiphyseal cancellous bone of a dog's tibial head: the shell-like structure of the cancellous bone is apparent. MMA-deplastified sample in the SEM. SEM of an air-dried specimen of a deplastified longitudinal ground section cleaned with pressurized air and documented in the PSEM 500, 50 kV, 200 Å. Horizontal field width=650 µm

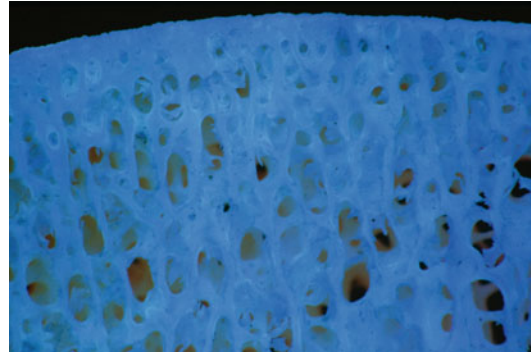


Fig. 2.12 Frontal section through a corroded femoral head of a 50-year-old man: the compact cartilage baseplate of a human femoral head is presented, supported by strong trabeculae comprising bone marrow spaces of distally increasing diameter. Ground section in incident fluorescent light. Horizontal field width=650 µm

the center of rotation of the femoral head, can be made (Fig. 2.13). The arterial vascularization of the epiphyses shows a lot of variables and is not yet comprehensively studied and documented. The arterial blood supply of the epiphysis plays a major role in all osteonecroses and is of utmost importance for the surgical approach for fracture treatment, i.e., the anterolateral approach for fractures of the lateral tibial condyle. The anatomy in that special topographical compartment was recently worked out (Hannouche et al. 2006). The deep branch of the medial femoral circumflex artery is considered of similar importance to

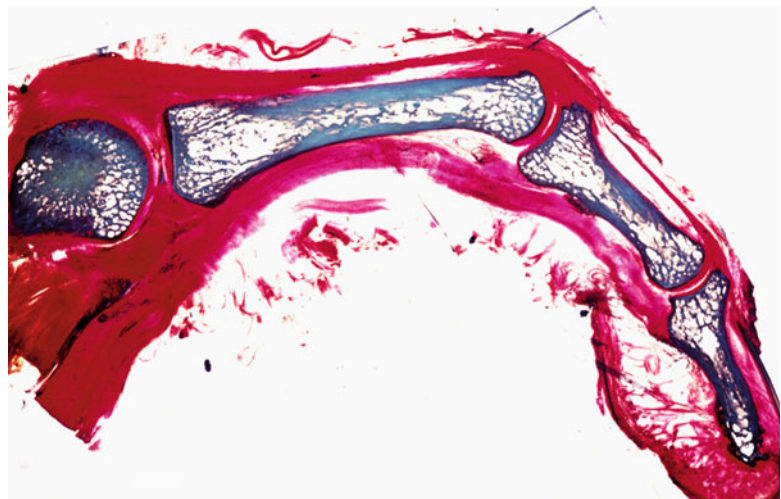


Fig. 2.11 Longitudinal section of a limb chain with joints, revealing the concave and convex delicate baseplate of the cartilage. Ground section of a human index finger, nondemineralized MMA-embedded ground section, basic fuchsin staining. Horizontal field width=10 cm



Fig. 2.13 Cross section through the center of rotation of a human femoral head: the orientation of the trabeculae resembles the balance wheel of a clock resisting strain acting upon it in a sagittal direction during walking. Two-millimeter-thick corroded cross section under the microscope. Horizontal field width=55 mm. Leitz: Aristophot

avoid or to understand the development of femoral head necrosis, i.e., for the surgical dislocation of the hip (Gautier et al. 2000; Ganz et al. 2001).

2.3 Metaphyseal Cancellous Bone

The shell-like structure of all bone subunits guarantees the largest possible surface area for resorption and, in the same way, its reinforcement. Toward the metaphysis, the shell-like walls of the cancellous bone become thinner and tubelike and well pronounced near the cortex of the proximal femur (Fig. 2.14) and along the metaphyseal cortical wall (Fig. 2.15). The thickness of a metaphyseal cancellous bone trabecula ranges between 80 and 100 μm , whereas the epiphyseal one is stronger and on average 250 μm thick. Sharpey's fiber bundles take a divergent spiral course inside the bone (Weidenreich 1922). The joint capsule, their reinforcements, ligaments, and tendons follow this principle, mainly in the metaphyseal compartment. A ligament or tendon substitute pulled through a drilled channel of a bone will

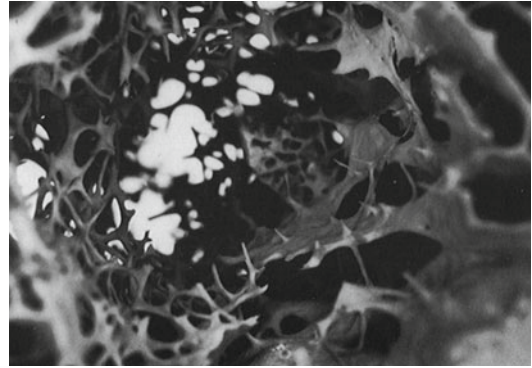


Fig. 2.14 View of the shell-like cancellous bone of the proximal metaphysis of a human femur: The medullary cavity is revealed with its wall-like shells. Corroded proximal femur of a 50-year-old man with resected femoral head and resected distal tube. Cleaned marrow spaces. Documentation was performed under the microscope using incident and transmitted light. Leitz: Macrozoom. Horizontal field width=90 mm

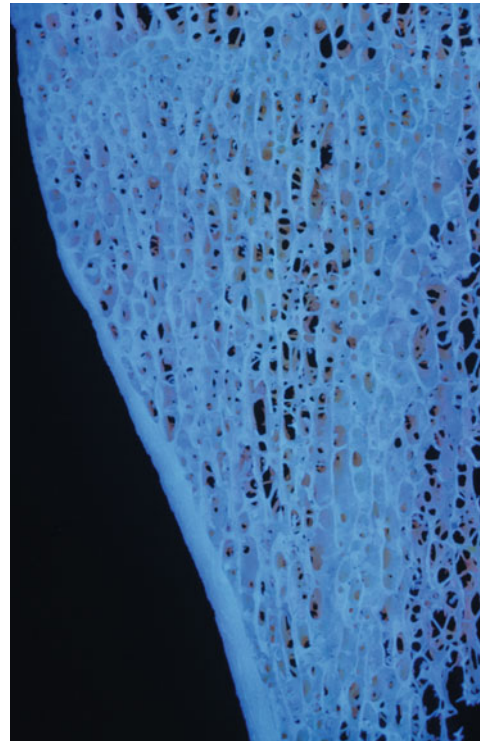


Fig. 2.15 View of a longitudinal frontal section of a human lateral femoral metaphysis. The shell-like cancellous bone comprises marrow spaces with a distally increasing diameter (1,000 μm). Corroded and cleaned sample from the lateral femoral metaphysis of a 50-year-old man, 2 mm thick, documented in incident fluorescent light. Horizontal field width=15 mm. Leitz: Makrozoom

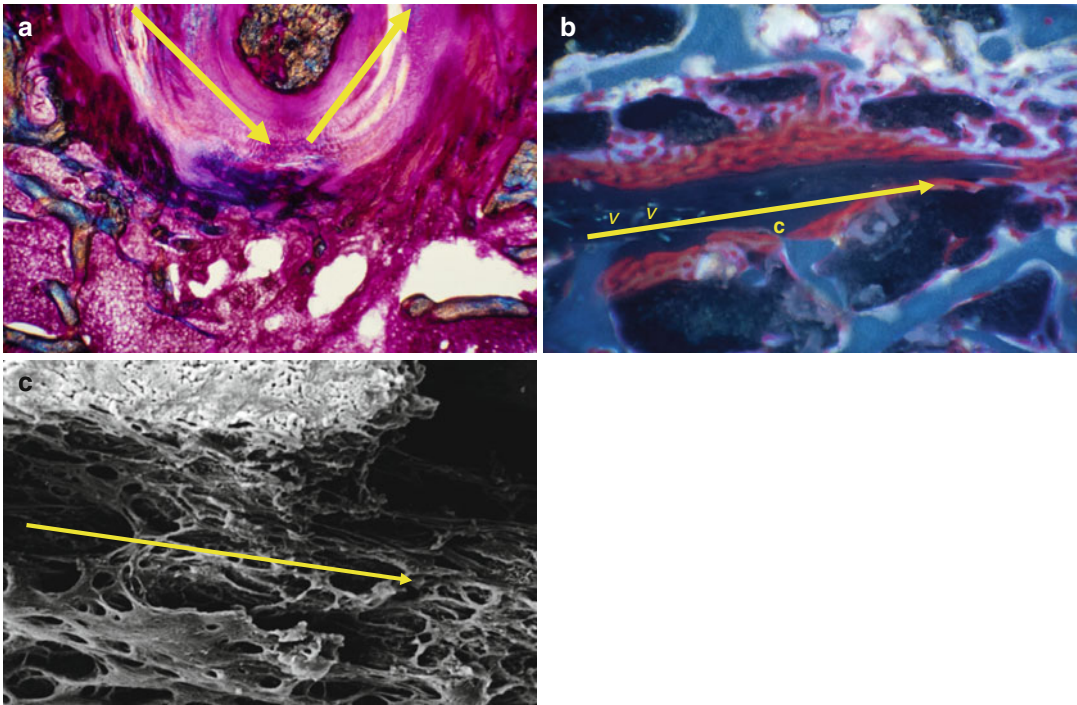


Fig. 2.16 (a) Cross section of a V-shaped drill hole anchorage of a ligament plastic: the cutis is pulled through a V-shaped drill hole (arrows); 6 weeks after the operation on a rabbit's tibial head, there is nearly no pronounced bony anchorage. MMA-embedded cross section in polarized transmitted light; alkaline fuchsine staining. Horizontal field width=12 mm. Leitz: Orthoplan; Apochromat 2.5x. (b) Cross section of a sandwich anchorage of a cutis plastic in a rabbit's tibial head: the sandwich gap was performed with a 300-µm saw blade by hand. The sandwich was closed by a miniscrew which pinched the cutis between bone surfaces (arrow). Three weeks after the operation, the cutis (c) is well vascularized and bony integrated from both sides. The vessels show a light

blue fluorescence (v); the bony anchorage took place in the second and third week (blue and red label); in the first week (yellow label), the recipient bed was reinforced. MMA-embedded cross section in incident fluorescent light; basic fuchsine staining. UV-filter. Horizontal field width=1,500 µm; Leitz: Orthoplan; Apochromat 4x. (c) Corroded cross section of (c) in the SEM: the newly formed bone is oriented along the path of fibers of the cutis (arrow), which has been removed by corrosion. The strong bony anchorage is well pronounced. Na_2O_2 processing, cleaning with gentle jet of a jet lavage; air-dried specimen. 200 Å gold sputtering. PSEM 500, 50 kV. Horizontal field width=150 µm

not be bony anchored by newly formed bone because the fibers converge, concentrating stress instead of distributing it (Draenert et al. 1981). The principle of a divergent course should be considered for the replantation operation, for

which there are principally two possibilities: the sandwich technique, (Fig. 2.16a–c; Draenert et al. 1981) or the bone dowelling technique, i.e., the bone–tendon–bone procedure replacing the ACL in the knee joint (Fig. 2.17a–e).

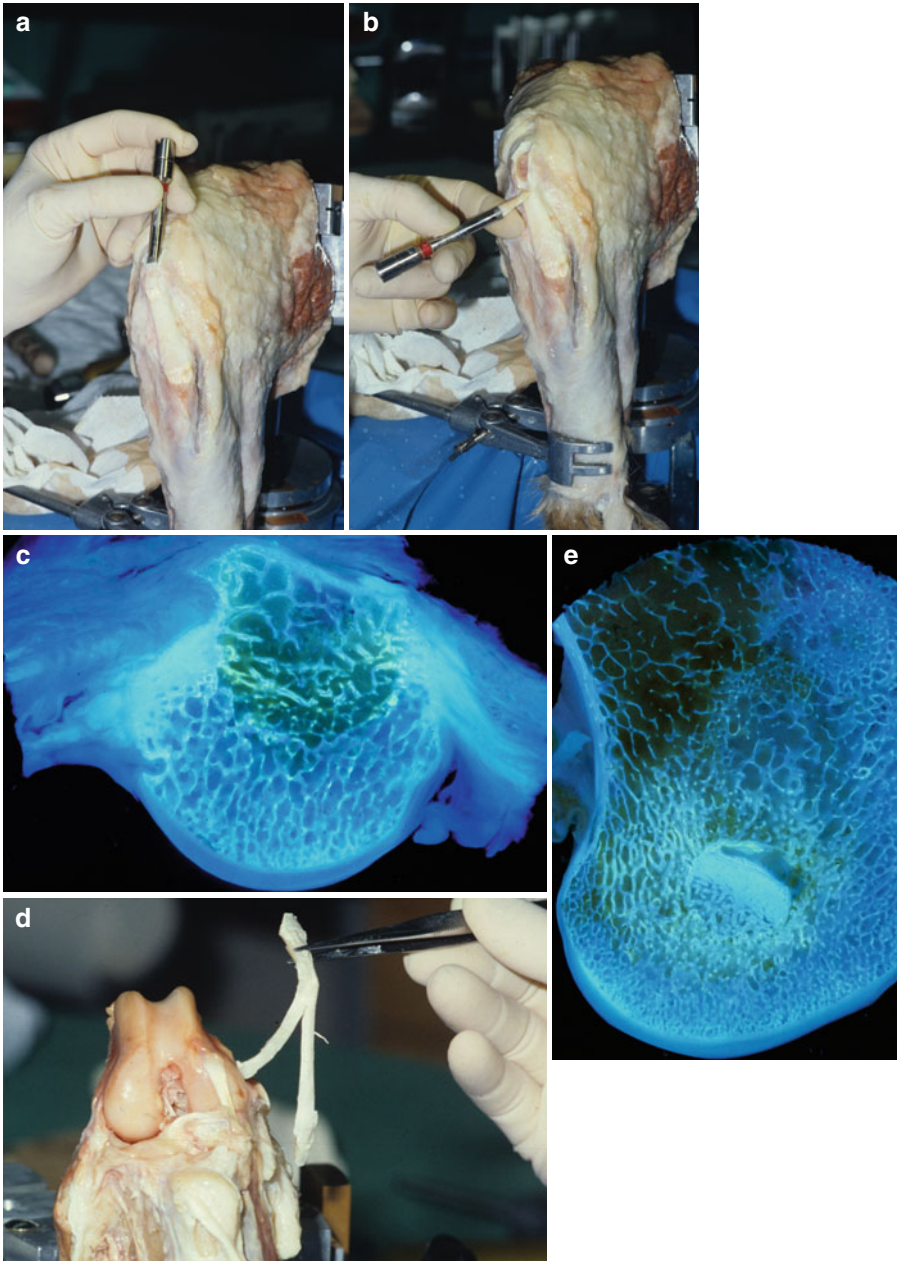


Fig. 2.17 (a, b) Animal experiment (Gerber, London) in a shepherd dog with the SDI procedure: a very precise wet-grinding process gathers the bone-tendon-bone graft. Preoperative planning in a dog's cadaver bone, just before the patellar tendon is cut. Leica: Kodak prof. 64. (c) Cross section through the dog's patella: a press-fit graft, gathered from the iliac crest and bony healed after 4 weeks, refills the donor bed. Fresh cross section in incident fluorescent light reveals the *yellow label* of the first and second postoperative week. Horizontal field width=22.5 mm. ZOW: *HIIFL* high intensity incident fluorescent light. (d) Double bundle plastic using the

outside-in technique in a preoperative dog's cadaver planning: the patellar tendon, as well as the bony shell of the tuberositas patellae, is split; both bundles are anchored in the tibial head and twisted 30–45°. (e) Bony integration of the patellar bone plug revealing the sandwich incorporation of the fiber layer in the ground canal of the lateral femoral condyle. Insertion was performed in a press-fit manner using the SDI technique. A fresh sagittal section in incident fluorescent light reveals the *yellow label* of the first and second postoperative week. Horizontal field width=19 mm. ZOW: *HIIFL* high intensity incident fluorescent light

References

- Becerra J, Andrades JA, Guerado E et al (2010) Articular cartilage: structure and regeneration. *Tissue Eng* 16:617–627
- Cameron CHS, Gardner DL, Longmore RB (1976) The preparation of human articular cartilage for SEM. *J Microsc* 108:1–12
- Chan SM, Neu CP, Duraine G et al (2010) Atomic force microscope investigation of the boundary-lubricant layer in articular cartilage. *Osteoarthritis Cartilage* 18:956–963
- Clarke IC (1971a) Human articular surface contours and related surface depression. Frequency studies. *Ann Rheum Dis* 30:15–23
- Clarke IC (1971b) A method for the replication of the articular cartilage surfaces suitable for the scanning electron microscope. *J Microsc* 93:67–71
- Clarke IC (1971c) Surface characteristics of human articular cartilage. A SEM study. *J Anat* 108:23–30
- Davies VD, Barnett CH, Cochrane W et al (1962) Electron microscopy of articular cartilage in the young adult rabbit. *Ann Rheum Dis* 21:11–22
- Draenert Y, Draenert K (1979) Freeze-drying of articular cartilage. *Scanning* 2:57–71
- Draenert K, Draenert Y, Springorum HW et al (1981) Histo-Morphologie des Spongiosadefektes und die Heilung des autologen Spongiosatransplantates. In: Cotta H, Martini AK (eds) *Implantate und Transplantate in der Plastischen und Wiederherstellungschirurgie*. Springer, Berlin
- Draenert K, Draenert Y, Bombelli R et al (2002) La guarigione primaria della cartilagine e dell'osso spugnoso ed il suo significato clinico. In: Pipino F (ed) *G I O T* 28:531–539
- Ganz R, Gill TJ, Gautier E et al (2001) Surgical dislocation of the adult hip. A technique with full access to the femoral head and acetabulum without the risk of avascular necrosis. *J Bone Joint Surg* 83-B:1119–1124
- Gautier E, Ganz K, Krügel N et al (2000) Anatomy of the medial femoral circumflex artery and its surgical implications. *J Bone Joint Surg* 82-B:679–683
- Ghadially FN, Roy S (1969) *Ultrastructure of synovial joints in health and diseases*. Livingstone, London, pp 40–86
- Ghadially FN, Ghadially JA, Oryschak AF et al (1976) Experimental production of ridges on rabbit articular cartilage. *J Anat* 121:119–132
- Ghadially FN, Thomas I, Oryschak AF et al (1977) Long-term results of superficial defects in articular cartilage. *J Pathol* 121:213–222
- Hannouche D, Duparc F, Beaufils P (2006) The arterial vascularization of the lateral tibial condyle: anatomy and surgical application. *Surg Radiol Anat* 28:38–45
- Hunter W (1743) Of the structures and diseases of articulating cartilage. *Philos Trans R Soc Lond (Biol)* 42:514–521
- Ranvier L (1873) Quelques faits relatifs au développement du tissu osseux. *Comptes rendus Acad Sci* 77: 1105–1109
- Rosenberg L, Hellmann W, Kleinschmidt AK (1970) Macromolecular models of protein polysaccharides from bovine nasal cartilage based on electron microscopic studies. *J Biol Chem* 245:4123–4130
- Rosenberg L, Hellmann W, Kleinschmidt AK (1975) Electron microscopic studies of proteoglycan aggregates from bovine articular cartilage. *J Biol Chem* 250:1877–1883
- Schenk R (1978) Histomorphologische und physiologische Grundlagen des Skelettwachstums. In: Weber BG, Brunner Ch, Freuler F (eds) *Die Frakturbehandlung bei Kindern und Jugendlichen*. Springer, Berlin
- Venn M, Maroudas A (1977) Chemical composition and swelling of normal and osteoarthritic femoral head cartilage. I. Chemical comp. *Ann Rheum Dis* 36:121–129
- Weidenreich F (1922) Über die Beziehungen zwischen Muskelapparat und Knochen und dem Charakter des Knochengewebes. *Erg H Anat Anz* 55:28–53
- Wolff J (1892) *Das Gesetz der Transformation der Knochen*. Hirschwald, Berlin

Autologous Resurfacing and Fracture Dowelling

A Manual of Transplantation Technique

Draenert, K.; Draenert, Y.; Pohlemann, T.; Regel, G.

2012, XII, 140 p. 189 illus., 149 illus. in color.,

Hardcover

ISBN: 978-3-642-24910-5